EHD2 is a mechanotransducer connecting caveolae dynamics with gene transcription

Stéphanie Torrino, Wei-Wei Shen, Cedric Blouin, Satish Kailasam Mani, Christine C. Viaris de Lesegno, Pierre Bost, Alexandre Grassart, Darius Köster, Cesar Augusto Valades-Cruz, Valérie Chambon, et al.

JCB Journal of Cell Biology

REPORT

EHD2 is a mechanotransducer connecting caveolae dynamics with gene transcription

Stéphanie Torrino[1,2,3]*, Wei-Wei Shen[1,2,3]*, Cédric M. Blouin[1,2,3], Satish Kailasam Mani[1,2,3], Christine Viaris de Lesegno[1,2,3], Pierre Bost[4,5], Alexandre Grassart[6], Darius Köster[7], Cesar Augusto Valades-Cruz[2,3,8], Valérie Chambon[2,3,8], Ludger Johannes[2,3,8], Paolo Pierobon[9], Vassili Soumelis[4], Catherine Coirault[10], Stéphane Vassilopoulos[10], and Christophe Lamaze[1,2,3]

Caveolae are small invaginated pits that function as dynamic mechanosensors to buffer tension variations at the plasma membrane. Here we show that under mechanical stress, the EHD2 ATPase is rapidly released from caveolae, SUMOylated, and translocated to the nucleus, where it regulates the transcription of several genes including those coding for caveolae constituents. We also found that EHD2 is required to maintain the caveolae reservoir at the plasma membrane during the variations of membrane tension induced by mechanical stress. Metal-replica electron microscopy of breast cancer cells lacking EHD2 revealed a complete absence of caveolae and a lack of gene regulation under mechanical stress. Expressing EHD2 was sufficient to restore both functions in these cells. Our findings therefore define EHD2 as a central player in mechanotransduction connecting the disassembly of the caveolae reservoir with the regulation of gene transcription under mechanical stress.

Introduction

Cells translate physical stimuli by mechanotransduction into biochemical signals that relay information from the cell surface to the nucleus, where gene expression is regulated. Mechanotransduction controls multiple cellular aspects including, but not limited to, cell growth, shape, or differentiation (Iskratsch et al., 2014). Abnormal cell responses to external and internal mechanical constraints are often associated with human pathologies such as heart diseases, myopathies, and cancer (DuFort et al., 2011). The underlying mechanisms integrating mechanosensing with mechanotransduction remain poorly understood.

Caveolae are 60–80-nm bulb-like plasma membrane invaginations discovered more than 60 years ago (Palade, 1953; Yamada, 1955). Caveolae are generated through tight association of caveolin 1 (Cav1) oligomers, its main structural component, and are stabilized by the assembly of cytoplasmic cavins into a coat-like structure around the caveolae bulb (Gambin et al., 2013; Ludwig et al., 2013; Stoeber et al., 2016). We established a new function of caveolae in mechanosensing and mechanoprotection in endothelial and muscle cells: under increase of membrane tension generated by cell swelling or stretching, caveolae flatten out immediately to provide additional surface area and prevent the rupture of the plasma membrane (Sinha et al., 2011). The central role of caveolae in cell mechanics has been confirmed in vivo (Cheng et al., 2015; Garcia et al., 2017; Lim et al., 2017) and has been extended to the muscle-specific isoform Cav3 (Cheng et al., 2015; Lo et al., 2015) and other cell types (Gervásio et al., 2011; Ariotti et al., 2014).

Here, we reveal that the Eps15 homology domain-containing 2 (EHD2) ATPase is released from mechanically disassembled caveolae and is subsequently translocated to the nucleus to mediate mechanotransduction through gene transcription. EHD2 is also required to maintain the caveolae reservoir at the plasma membrane under membrane tension variations. Thus, EHD2 plays a pivotal role in the cell adaptation to mechanical perturbations by connecting caveolae mechanosensing at the plasma membrane with the regulation of gene transcription.

Results and discussion

EHD2 is rapidly translocated from caveolae to the nucleus upon mechanical stress

The mechanical flattening of caveolae is immediately followed by the disassembly of caveolae and the release of caveolar proteins

[1]Membrane Dynamics and Mechanics of Intracellular Signaling Laboratory, Centre de Recherche, Institut Curie, PSL Research University, Paris, France; [2]Institut National de la Santé et de la Recherche Médicale (INSERM), U1143, Paris, France; [3]Centre National de la Recherche Scientifique, UMR 3666, Paris, France; [4]Laboratoire d'Immunologie Clinique, INSERM U932, Centre de Recherche, Institut Curie, Paris, France; [5]Department of Biology, École Normale Supérieure, PSL Research University, Paris, France; [6]Unité de Pathogénie Microbienne Moléculaire, INSERM 1202, Institut Pasteur, Paris, France; [7]Cell and Developmental Biology, Warwick Medical School Biomedical Sciences, Warwick University, Coventry, UK; [8]Endocytic Trafficking and Intracellular Delivery Laboratory, Centre de Recherche, Institut Curie, PSL Research University, Paris, France; [9]INSERM U932, Institut Curie, PSL Research University, Paris, France; [10]Sorbonne Université, INSERM, Institute of Myology, Centre of Research in Myology, UMRS 974, Paris, France.

*S. Torrino and W.-W. Shen contributed equally to this paper; Correspondence to Christophe Lamaze: christophe.lamaze@curie.fr.

including Cav1 and cavins (Sinha et al., 2011; Gambin et al., 2013). We hypothesized that the release of caveolae components into the cytosol could mediate mechanotransduction events (Nassoy and Lamaze, 2012; Lamaze et al., 2017). We monitored the fate of cavin1 and EHD2 because these two peripheral proteins of caveolae bear nuclear localization signals and can undergo nucleocytoplasmic shuttling (Pekar et al., 2012; Nassar and Parat, 2015). ATP hydrolysis drives EHD2 oligomerization at the neck of caveolae, where it controls their stability through anchoring to the actin cytoskeleton (Morén et al., 2012; Stoeber et al., 2012). Cavin1/PTRF is the first identified member of the cavin family that participates in the formation of the cytoplasmic coat of caveolae (Ludwig et al., 2013; Kovtun et al., 2014).

Under resting conditions, EHD2 was present at the plasma membrane of HeLa cells, where it colocalized with ∼50–60% of Cav1 puncta, as previously shown (Fig. S2 A; Morén et al., 2012; Stoeber et al., 2012). As expected, a fraction of EHD2 was present in the nucleus (Fig. 1 A; Pekar et al., 2012). Repeated cycles of cell stretching and relaxation led to a moderate (≈10%), albeit significant, increase of the EHD2 signal in the nucleus. A fraction of cavin1, which bears two nuclear localization signals, was also present in the nucleus at steady state. No further increase of nuclear cavin1 was measurable upon cyclic stretch (Fig. 1 B). We also followed the intracellular fate of EHD2 under acute disassembly of caveolae induced by hypo-osmotic shock (Sinha et al., 2011). After 5 min of hypo-osmotic shock (Hypo), we measured a significantly higher (≈45%) increase in EHD2 nuclear translocation. In contrast, Cav1 was not translocated to the nucleus upon mechanical stress (Figs. 1 C and S1 A). EHD2 nuclear translocation increased with the hypo-osmotic shock strength (Fig. S1 A). We followed EHD2 dynamics in live cells in 3D with lattice light sheet microscopy (Chen et al., 2014). During the course of the hypo-osmotic shock, the amount of nuclear EHD2 increased rapidly, reaching a plateau in ∼100 s (Fig. S1 C and Video 1). Upon return to iso-osmotic conditions, the caveolae reservoir is rapidly reassembled at the plasma membrane (Sinha et al., 2011). Under this condition (Rec), the amount of nuclear EHD2 decreased to a level slightly below steady state (Figs. 1 C and S1 A).

We quantified the amount of endogenous EHD2 present in the nuclear, cytoplasmic, and membrane fractions of cellular protein extracts from mouse lung endothelial cells (MLECs). At steady state, EHD2 was distributed between the nuclear, cytoplasmic, and membrane fractions of MLEC WT cells having caveolae (Fig. 1 D). Hypo-osmotic shock led again to a significant increase of EHD2 nuclear content and a concomitant decrease in the membrane fractions, whereas the cytoplasmic fraction remained constant. In contrast, the initial distribution of EHD2 was not significantly changed by hypo-osmotic shock in MLEC Cav1$^{-/-}$ cells devoid of caveolae, indicating that functional caveolae were required for EHD2 nuclear translocation induced by mechanical stress (Fig. 1 D). Similarly, a lack of EHD2-mCherry nuclear translocation was observed in HeLa Cav1$^{-/-}$ cells (Fig. S1 B). In these cells, the amount of nuclear EHD2-mCherry was higher, suggesting that the association of EHD2 with caveolae at the plasma membrane prevents its nuclear translocation. Finally, total internal reflection microscopy (TIRF) live-cell imaging showed that dually labeled Cav1 and EHD2 puncta synchronously disappeared from the plasma membrane with the same amplitude under hypo-osmotic shock, implying that EHD2 was released during caveolae disassembly (Fig. S2 A). These observations clearly demonstrate that the mechanical disassembly of caveolae at the plasma membrane results in the translocation of EHD2 to the nucleus.

Mechanical stress results in EHD2 SUMOylation

We next investigated which possible posttranslational modifications of EHD2 could be associated with its mechanical release from caveolae. EHD2 was reported to be SUMOylated by SUMO1 (small ubiquitin-like modifier) on Lys^{315}, which, when mutated, resulted in EHD2 nuclear accumulation (Pekar et al., 2012). Protein SUMOylation has clearly been associated with nucleocytoplasmic transport and the response to different types of stresses, including osmotic stress (Geiss-Friedlander and Melchior, 2007; Enserink, 2015). We first explored the interaction between endogenous EHD2 and SUMO using the proximal ligation assay (PLA; Söderberg et al., 2006). In Hs578T cells, which present substantial amounts of caveolae (see Fig. 5, A–C), PLA confirmed that endogenous EHD2 was SUMOylated by SUMO1 (Fig. S2 B). At steady state, a significant amount of EHD2-SUMO1 was localized in the nucleus and to a lesser extent in the cytoplasm and at the plasma membrane. Hypo-osmotic shock did not increase EHD2 SUMOylation but led to a significant relocation of EHD2-SUMO1 in the nucleus. We also analyzed the possible SUMOylation of EHD2 by SUMO2/3 and found minimal levels of EHD2-SUMO2/3 under resting conditions (Fig. 2 A). Unlike SUMO1, however, hypo-osmotic shock led to a general increase of the cellular amount of EHD2-SUMO2/3, with a significant increase in nuclear EHD2-SUMO2/3 (Fig. 2, A and B). We confirmed EHD2 SUMOylation biochemically by transfecting EHD2-GFP in HeLa cells stably expressing His-SUMO2/3. The amount of EHD2-SUMO2/3, minimal under resting conditions, increased again after hypo-osmotic shock (Fig. 2 C).

We also measured EHD2 SUMOylation after mechanical stress release when the initial number of caveolae has fully recovered. We found a significant decrease of both EHD2-SUMO1 and EHD2-SUMO2/3, especially in the nucleus, suggesting that EHD2 deSUMOylation had occurred (Figs. 2 A and S2 B). Finally, we analyzed the EHD2 SUMOylation deficient mutant KK315-316AA, previously shown to accumulate in the nucleus, implying that EHD2-SUMOylation controlled EHD2 nuclear exit (Pekar et al., 2012). The EHD2-KK315-316AA mutant disappeared synchronously with Cav1 from the plasma membrane under hypo-osmotic shock but was unable to relocate to caveolae after shock release (Fig. S2 A). Finally, no increase in EHD2-SUMOylation was measurable in MLEC Cav1$^{-/-}$ cells (Fig. 2 D), indicating that the pool of EHD2 that is SUMOylated under hypo-osmotic shock is the pool that was initially associated with caveolae at the plasma membrane. Together, these data show that the cycle of EHD2 SUMOylation is controlled by mechanical stress and plays a key role in the nucleocytoplasmic shuttling of EHD2.

EHD2 controls gene transcription under mechanical stress

To address the functional significance of EHD2 nuclear translocation, we used gene set enrichment analysis (GSEA; Subramanian et al., 2005) to compare the transcriptome of Hs578T cells

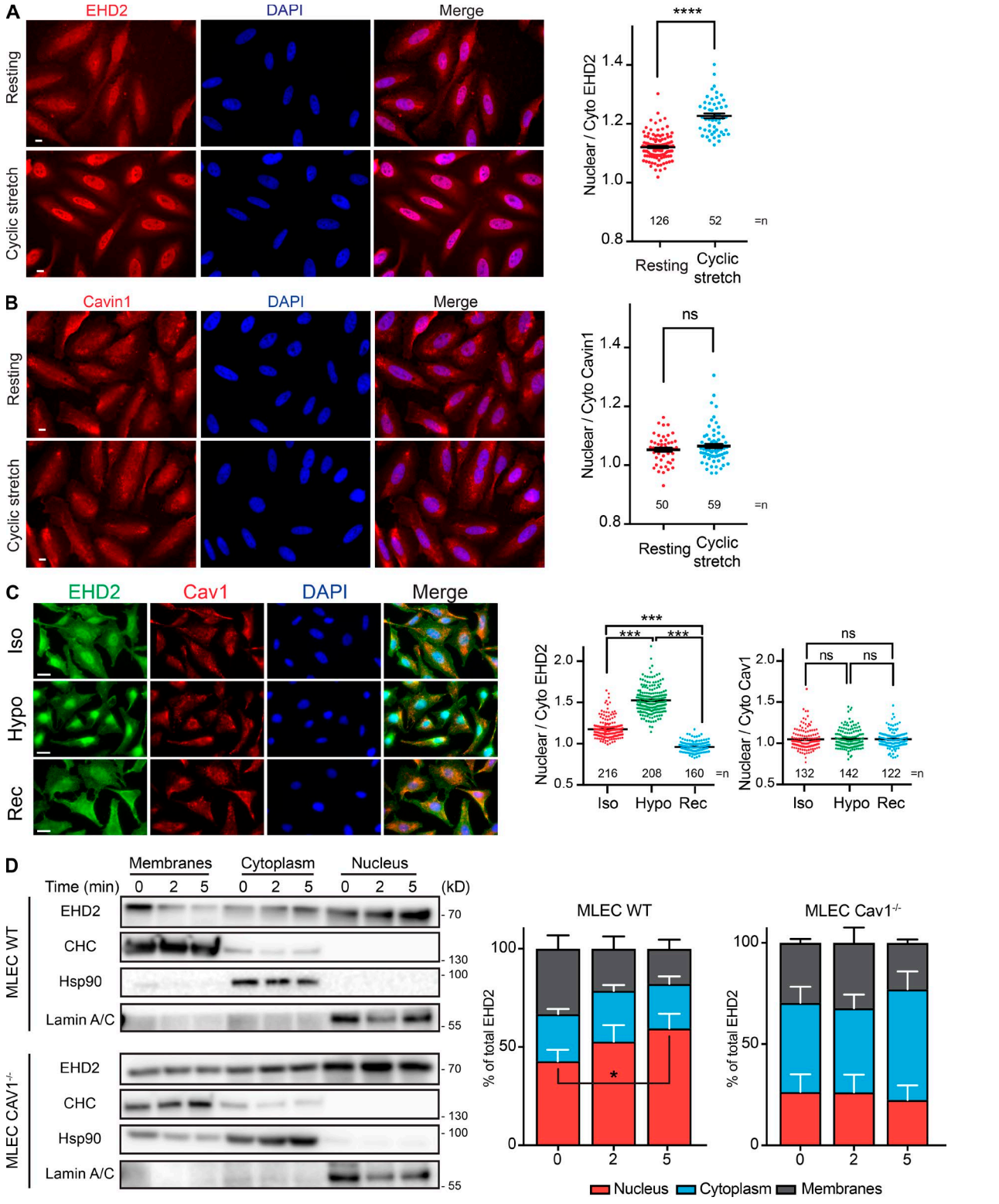

Figure 1. **Mechanical stress induces EHD2 nuclear translocation. (A and B)** Representative wide-field immunofluorescence (left) and quantification (right) of the nuclear translocation of endogenous EHD2 (A) but not cavin1 (B) in HeLa cells after 30 min of cyclic stretch. **(C)** Representative wide-field immunofluorescence (left) and quantification (right) of endogenous EHD2 and Cav1 localization in HeLa cells under resting (Iso), after 5 min of 30 mOsm hypo-osmotic shock (Hypo), and 5 min after return to iso-osmotic conditions (Rec). **(D)** Immunoblot analysis (left) and quantification (right) of equal amounts of nuclear, cytoplasmic and cell membrane extracts after hypo-osmotic shock for the indicated times in MLEC cells having caveolae (WT) or not ($Cav1^{-/-}$). Scale bar = 10 µm; $n \geq 3$ independent experiments; *, $P < 0.05$; ***, $P < 0.001$; ****, $P < 0.0001$; in A and B, two-tailed *t* test; data are representative of three experiments, mean ± SEM; in C, Bonferroni's multiple comparison test; data are mean ± SEM; numbers of cells are indicated on the graphs; in D, Dunn's multiple comparison test; $n = 3$; data are mean ± SEM.

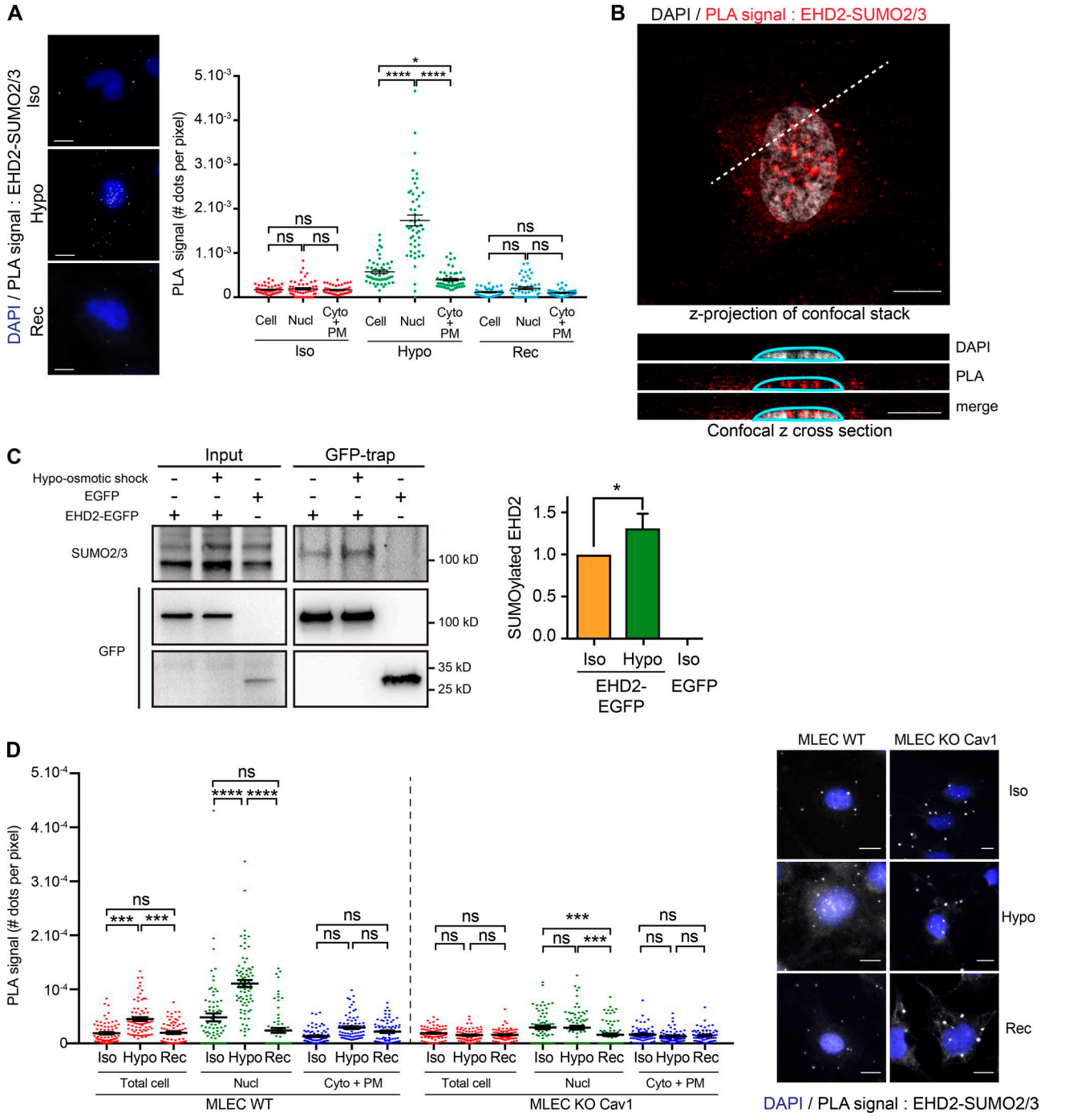

Figure 2. **EHD2 is SUMOylated by SUMO2/3 upon mechanical stress. (A)** Representative wide-field fluorescence (left) and quantification (right) of in situ PLA experiments in Hs578T cells monitoring EHD2 and SUMO2/3 interaction in the whole cell (Cell), the nucleus (Nucl), and the cell minus the nucleus (Cyto + plasma membrane) under resting (Iso, *n* = 51), under hypo-osmotic (Hypo, *n* = 51), and after return to iso-osmotic (Rec, *n* = 50) conditions. **(B)** Representative z-projection (average intensity) of a confocal stack of a PLA experiment monitoring EHD2 and SUMO2/3 interaction (red signal) in MLEC cells 5 min after 30 mOsm hypo-osmotic shock. A confocal z cross section along the dashed line shows localization of PLA spots in the nucleus (DAPI; gray). **(C)** Immunoblot analysis (left) and quantification (right; SUMO2/3 level normalized to GFP) of EGFP-EHD2 SUMOylation by SUMO2/3 in immunoprecipitates from stable HeLa His-SUMO2/3 cells transfected with EHD2-EGFP or EGFP under Iso and Hypo conditions. **(D)** Same PLA experiments as in A performed in MLEC WT (Iso, *n* = 76; Hypo, *n* = 77; Rec, *n* = 72) or Cav1$^{-/-}$ cells (Iso, *n* = 75; Hypo, *n* = 75; Rec, *n* = 75). Scale bar = 10 µm; *, P < 0.05; ***, P < 0.001; ****, P < 0.0001; in A and D, Dunnett's multiple comparison test, data are representative of three experiments, mean ± SEM; in C, repeated measures one-way ANOVA; data are mean ± SEM.

depleted or not from EHD2 and subjected to cyclic stretch for 30 min at 0.5 Hz. GSEA showed that cyclic stretching resulted in the positive enrichment of gene sets involved in hallmark signaling pathways such as TNF-α, K-Ras, and receptor interaction with the extracellular matrix (Fig. 3 A; http://microarrays.curie.fr/). When EHD2 was silenced, the gene set regulation observed under mechanical stress was lost. In addition, distinct gene sets related to cell cycle, cell division, and cell-cycle checkpoints were also

negatively regulated. Although cyclic stretching did not result in major changes in the pattern of gene set enrichment modified by EHD2 silencing, differences in the regulation of gene sets encoding transcription factors and cell division were further shown.

We next measured mRNA levels of caveolae constituents by reverse-transcription quantitative PCR (RT-qPCR) in HeLa cells under mechanical stress. Cyclic stretch led to a significant decrease of caveolae constituent transcripts, i.e., Cav1, Cav2, cavin1, and cavin2, without affecting transcripts of flotillin-1 (Flot1), a related membrane protein assembling microdomains distinct from caveolae at the plasma membrane (Fig. 3 B). Similar data were obtained under hypo-osmotic shock (Fig. S2 C). Importantly, no modification of transcript levels was detected in cells depleted of EHD2 (Figs. 3 B and S2 C), and a siEHD2-resistant variant fully rescued the regulation of caveolae constituent genes in EHD2-depleted cells (Fig. S2 C). The mechanical regulation of caveolae constituent gene transcription by EHD2 was no longer observed in Cav1-depleted cells, confirming that the nuclear translocation of EHD2 and its impact on gene transcription requires the disassembly of functional caveolae (Fig. S2 D). Finally, the repression activity of EHD2 on transcription was mediated by Krüppel-like factor 7 (KLF7) and modulator of KLF7 activity (MOKA; Fig. 3 C), two known partners of EHD2-regulated transcription (Pekar et al., 2012). Interestingly, KLF7 was found to bind to several enhancers of caveolae constituent genes in different cell lines (Fig. S2 E).

EHD2 stabilizes caveolae during membrane tension variations

We next analyzed the role of EHD2 in caveolae dynamics using TIRF and found, as previously published (Morén et al., 2012; Stoeber et al., 2012; Yeow et al., 2017), that EHD2 depletion did not change the number of Cav1 spots present at the plasma membrane under resting conditions. Whereas EHD2 depletion had no effect on the extent of caveolae disassembly under hypo-osmotic shock, the reassembly of caveolae, which normally occurs immediately after the release of mechanical stress, was significantly reduced (Fig. 3 D). Expression of the dominant-negative EHD2-T72A mutant (unable to bind ATP) also reduced caveolae recovery after mechanical stress release. Conversely, expression of wild-type EHD2, EHD2-I157Q constitutively active mutant (with accelerated ATP hydrolysis), or a siEHD2-resistant variant allowed caveolae reassembly (Figs. 3 E and S3 A). Finally, depletion or overexpression of Pacsin2 and filamin A, proteins that link caveolae to the actin cytoskeleton, did not affect the reassembly of caveolae after mechanical stress release (Fig. S3, B and C).

We next examined the role of EHD2 under membrane tension variations by measuring the effective membrane tension using the tether pulling technique as described previously (Sheetz, 2001; Sinha et al., 2011). HeLa cells were first exposed to a 5-min hypo-osmotic shock (150 mOsm) to increase membrane tension, and then to iso-osmolarity for 5 min to allow the return of membrane tension to homeostasis (Rec condition). By recording the mean variations of the tether force ΔF over the initial force F_{iso} measured in isotonic conditions, we found, as expected for cells having functional caveolae (Sinha et al., 2011), that the increase of membrane tension induced by hypo-osmotic shock was buffered, as F_{hypo} remained almost identical to F_{iso} (Fig. 3 F). When cells were depleted of EHD2, there was a slight but not significant increase in membrane tension, in agreement with our finding that EHD2 depletion did not change the extent of caveolae disassembly induced by hypo-osmotic shock (Fig. 3 F). 5 min after return to iso-osmolarity (Rec), the membrane tension of control cells had not yet returned to the initial value measured before stress, as indicated by the negative value of the tether force ΔF. In EHD2-depleted cells, however, we measured a drastically smaller value of membrane tension, indicating a stronger delay in the return to membrane tension homeostasis (Fig. 3 F). We also found that repeated cycles of stretching and relaxation led to a slight but significant decrease of the number of caveolae at the plasma membrane in cells depleted of EHD2 (Fig. 3 G). Altogether, these data indicate that EHD2 is required for maintaining a functional reservoir of caveolae at the plasma membrane, which buffers the variations of membrane tension during mechanical stress.

Loss of EHD2 expression impairs caveolae mechanosensing and gene transcription

Low EHD2 expression was recently reported in several solid tumors (Li et al., 2013; Shi et al., 2015; Yang et al., 2015; Liu et al., 2016). Whether low EHD2 expression was also associated with defects in caveolae stabilization and nuclear translocation was not investigated in those studies. Given the importance of the mechanical microenvironment in tumor progression (DuFort et al., 2011) and the association of Cav1 with tumorogenesis (Goetz et al., 2008; Lamaze and Torrino, 2015), we investigated caveolae mechanics in breast cancer cell lines. We measured EHD2 mRNA levels in several normal and cancerous breast epithelial cell lines and selected Hs578T and MDA-MB-436, two triple-negative basal-like breast cancer cell lines that express high and minimal levels of EHD2 transcripts, respectively. Immunoblot analyses confirmed similar amounts of Cav1 and cavin1 proteins in Hs578T and MDA-MB-436 cells, whereas EHD2 was expressed in Hs578T but undetectable in MDA-MB-436 cells (Fig. 4 A).

We first investigated the dynamics of caveolae under mechanical stress by TIRF microscopy. In agreement with the disassembly of caveolae induced by higher membrane tension, we observed a rapid and significant decrease of Cav1 spots at the cell surface of Hs578T cells after exposure to a hypo-osmotic shock (Fig. 4 B). In contrast, the number of Cav1 spots remained identical in MDA-MB-436 cells (Fig. 4 C). However, when EHD2 was expressed in MDA-MB-436 cells, a strong decrease in cell surface Cav1 spot numbers was observed again under hypo-osmotic shock (Fig. 4 D).

We next addressed whether this defect in caveolae mechanosensing was also associated with defects in gene transcription regulation. MDA-MB-436 cells did not show any variation in the level of caveolae component transcription under mechanical stress, whereas the reexpression of EHD2, but not Cav1, restored this control (Fig. 4 E). Importantly, the restoration of this control required caveolae, as it was no longer observed when EHD2-transfected MDA-MB-436 cells were depleted of Cav1 (Fig. 4 E). Whereas cyclic stretch led to a decrease of caveolae component transcripts in Hs578T cells, EHD2 depletion suppressed this control (Fig. 4 F). Similar results were observed in cells depleted of Cav1. Altogether, these data confirm that

A

gene set names	Gene enrichment		
	Stretch	siEHD2	siEHD2 + stretch
ECM-receptor interaction	+		
AHR	+		
SRF	+		
Kras down	+		
TNFα signaling	+	+	+
Kras up		+	+
Hypoxia		+	+
Unfolded protein response		+	+
Apoptosis		+	+
STK33 up		+	+
E2F targets		-	-
E2F transcription factors			-
G2M checkpoints		-	-
Cell cycle		-	-
Cell division		-	
Beta catenin up		-	-

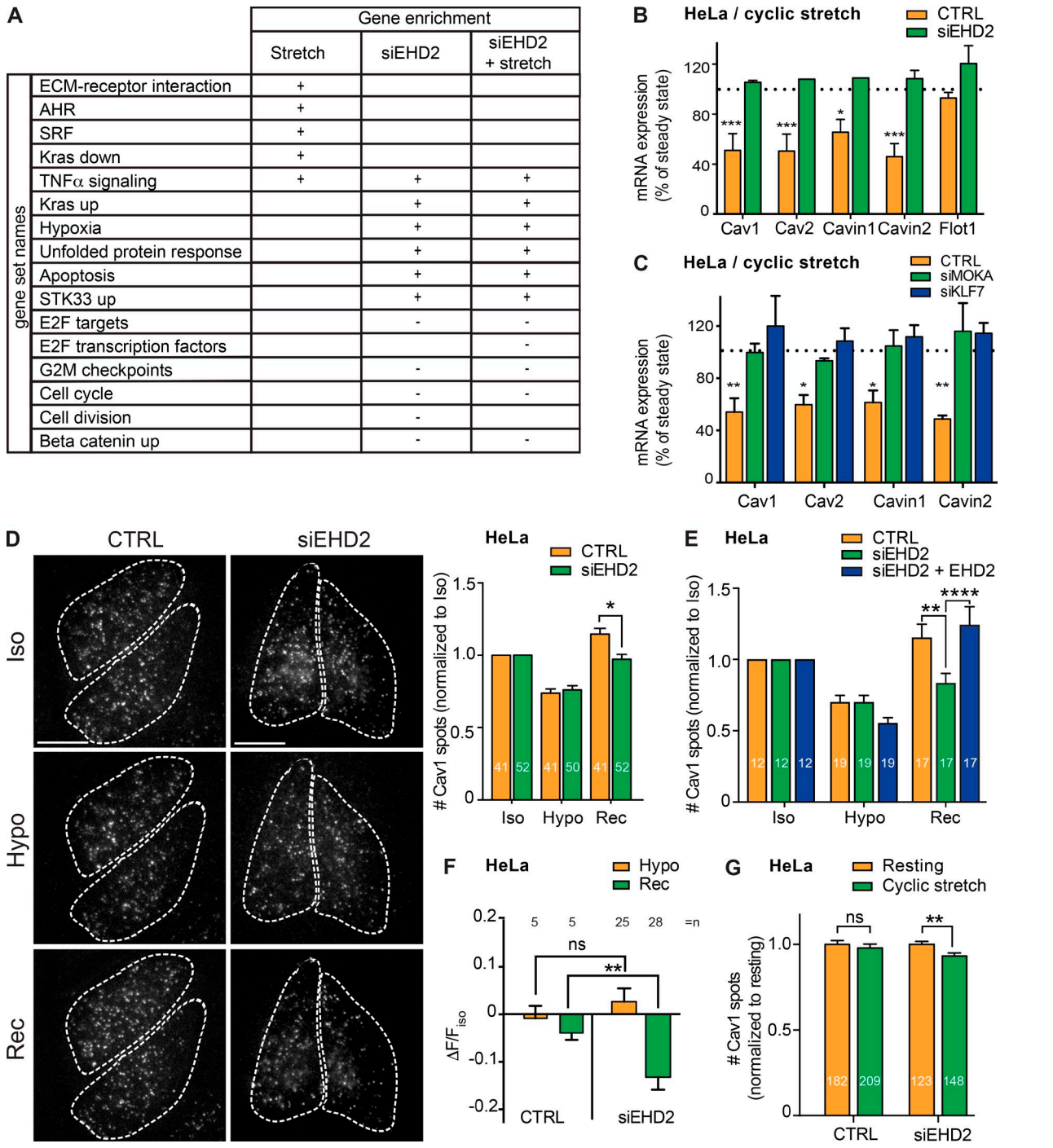

Figure 3. **EHD2 is required for the stabilization of caveolae and the control of gene transcription during tension variations at the plasma membrane. (A)** GSEA was performed to identify gene sets positively (+) or negatively (–) enriched by cyclic stretch in Hs578T cells depleted or not from EHD2. **(B)** Quantification of Cav1, Cav2, cavin1, cavin2, and flotillin-1 (Flot1) mRNA levels in HeLa cells transfected with control siRNA (CTRL) or siEHD2, after 30 min cyclic stretch. **(C)** Quantification of Cav1, Cav2, cavin1, and cavin2 mRNA levels in HeLa cells transfected with control siRNA (CTRL), siMOKA, or siKLF7 after 30 min cyclic stretch. **(D)** Representative TIRF images (left) and quantification (right) of changes in cell-surface Cav1 spot numbers in control siRNA (CTRL) or siEHD2-transfected Cav1-EGFP HeLa cells under resting (Iso), under hypo-osmotic (Hypo), and after return to iso-osmotic (Rec) conditions. Cells are delineated by dashes. **(E)** Quantification of changes in cell-surface endogenous Cav1 spot numbers in HeLa cells depleted (siEHD2) or not (CTRL) for EHD2 and transfected or not with EHD2-EGFP (+ EHD2) under Iso, Hypo, and Rec conditions. **(F)** Relative changes of the mean tether force under Hypo and Rec conditions in control siRNA (CTRL) and siEHD2 HeLa cells. **(G)** Quantification of cell surface Cav1 spot numbers at rest and after 30 min cyclic stretch in control siRNA (CTRL) or siEHD2 transfected HeLa cells. *, P < 0.05; **, P < 0.001; ***, P < 0.001; ****, P < 0.0001; two tailed *t* test. In B and C, Bonferroni's multiple comparison test; *n* = 3 independent experiments; in D–G, two-way ANOVA and Tukey's multiple comparisons test; *n* = 3; data are mean ± SEM. Numbers of cells are indicated on histogram bars. Scale bar = 10 µm.

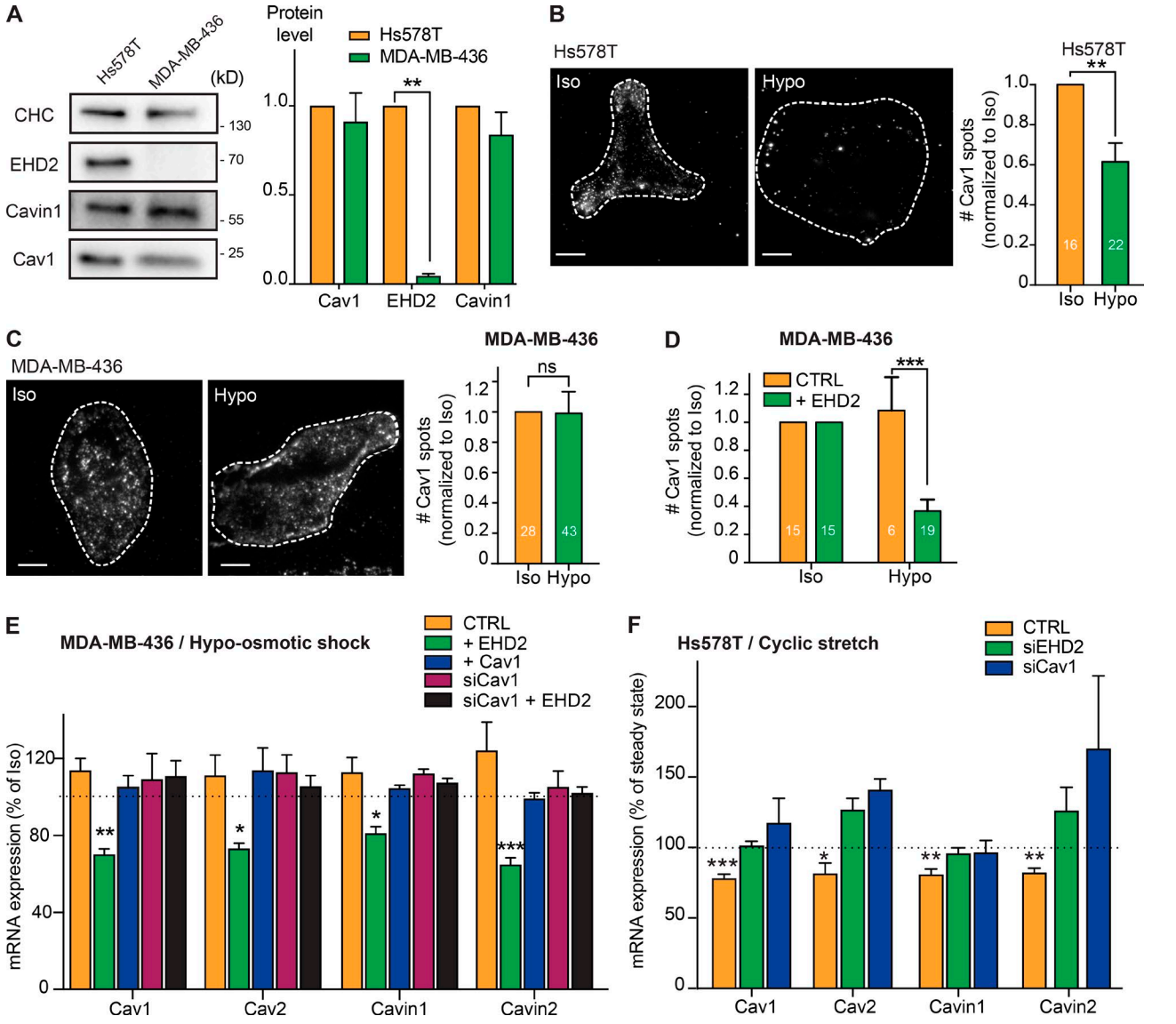

Figure 4. **Loss of EHD2 expression impairs caveolae mechanosensing and gene transcription in breast cancer cells. (A)** Immunoblot (left) and quantification (right) of EHD2, Cav1, and cavin1 protein levels normalized to CHC in Hs578T and MDA-MB-436 cells. **(B and C)** Representative TIRF images of changes in cell surface Cav1 spot numbers (left) and quantification (right) under resting (Iso) and hypo-osmotic (Hypo) conditions in Hs578T (B) or MDA-MB-436 (C) cells. Cells are delineated by dashes. Scale bar = 10 µm. **(D)** Quantification of changes in cell surface Cav1 spot numbers in MDA-MB-436 cells transfected or not (CTRL) with EHD2-EGFP under Iso and Hypo conditions. **(E)** Quantification of Cav1, Cav2, cavin1, and cavin2 mRNA levels in MDA-MB-436 cells transfected or not (CTRL) with EHD2 or Cav1 and in MDA-MB-436 cells depleted for Cav1 (siCav1) and transfected or not by EHD2 under hypo-osmotic conditions. **(F)** Quantification of Cav1, Cav2, cavin1, and cavin2 mRNA levels in Hs578T cells transfected with control siRNA (CTRL), siEHD2, or siCav1 after 30 min of cyclic stretch. For all panels, $n \geq 3$ independent experiments; mRNA levels are compared with resting conditions (dotted line); *, $P < 0.05$; **, $P < 0.01$; ***, $P < 0.001$; two tailed *t* test; data are mean ± SEM; numbers of cells are indicated on histogram bars.

functional caveolae are required for the mechanical control of gene transcription by EHD2.

To better understand how EHD2 controls the caveolae reservoir in breast cancer cells, we analyzed the ultrastructure of caveolae on unroofed cells using metal replica EM. Consistent with high Cav1 and EHD2 expression, Hs578T cells displayed numerous budded caveolae (Fig. 5, A–C). In contrast, MDA-MB-436 cells, which lack EHD2, presented very few caveolae, if any, and most membrane invaginations were clathrin-coated pits (Fig. 5, D–F). Cav1 immunogold labeling on standard transmission electron micrographs confirmed the absence of caveolar invaginations in MDA-MB-436 cells but revealed a significant amount of Cav1 proteins present at the plasma membrane (Fig. 5 J). In contrast, Cav1 proteins were always associated with bona fide caveolar invaginations in Hs578T cells. These results most likely explain the lack of caveolae disassembly observed in MDA-MB-436 cells (Fig. 4 C), because the Cav1 signal does not correspond to caveolar invaginations but to Cav1 clusters that are unlikely to flatten out under mechanical stress. Expressing EHD2 in MDA-MB-436 cells was sufficient to reconstitute the reservoir of caveolae at the plasma membrane (Fig. 5, G, H and I). EHD2 has not been involved in caveolae assembly (Morén et al., 2012; Stoeber et al.,

2012; Hoernke et al., 2017); therefore, it was unexpected that MDA-MB-436 breast cancer cells do not have caveolae, because their level of Cav1 and cavin1 expression is similar to that of Hs578T cells (Fig. 4 A). Our data strongly suggest that the absence of caveolae in breast cancer cells lacking EHD2 may represent a long-term consequence of the inability to stabilize the reservoir of caveolae under the changing mechanical environment experienced by cancer cells in the tumor mass. In this context, it is interesting that a recent study showed that EHD proteins (1, 2, and 4) are functionally redundant and that only the absence of all three EHDs results in loss of caveolae under mechanical stress (Yeow et al., 2017).

We and others have established caveolae as key mechanosensors (Gervásio et al., 2011; Sinha et al., 2011; Ariotti et al., 2014; Cheng et al., 2015; Lo et al., 2015). We reveal here that caveolae are also mechanotransducers, and that EHD2 is central to this new function. On the one hand, we show that ATP binding to EHD2 is required for assembling and stabilizing the reservoir of caveolae at the cell surface against the variations of membrane tension induced by mechanical stress. ATP binding allows EHD2 insertion into the plasma membrane, whereas ATP hydrolysis, possibly regulated by membrane curvature, is involved in EHD2 release (Hoernke et al., 2017). It is tempting to propose that caveolae flattening could trigger ATP hydrolysis by EHD2 and thereby its release from the plasma membrane. On the other hand, we show that the release of EHD2 from mechanically disassembled caveolae is rapidly followed by EHD2 nuclear translocation, where it regulates gene transcription. EHD2 SUMOylation, which is induced by mechanical stress, is a major regulator of EHD2 nucleocytoplasmic shuttling. Force-induced phosphorylation of Cav1 has been reported to regulate gene transcription of caveolae constituent biogenesis (Joshi et al., 2012). Our new results on EHD2 SUMOylation further illustrate the key role of posttranslational modifications in the caveolae response to mechanical stress. EHD2, which combines both mechanosensing and mechanotransducing activities, plays a central role in the mechanical cell response (Fig. 5 K).

Recent evidence shows that mechanical forces from both the tumor mass and its microenvironment can control cancer cells activity in vivo (DuFort et al., 2011; Fernández-Sánchez et al., 2015). Our study is the first report of a defect in caveolae mechanosensing and mechanotransduction in cancer cells and emphasizes the importance of revisiting the classic cellular functions of caveolae and their constituents through their new role in cell mechanics.

Materials and methods

Antibodies and reagents

The following commercially available antibodies were used for Western blotting: mouse monoclonal antibodies against clathrin heavy chain (CHC; BD Biosciences; 610500), lamin A/C (Santa Cruz Biotechnology; sc-7292), Hsp90 (Santa Cruz Biotechnology; sc-13119), EHD2 (Santa Cruz Biotechnology; sc-100724), dynamin (BD Biosciences; 610245), and filamin A (Chemicon; MAB1678); rabbit polyclonal antibodies against SUMO2/3 (Cell Signaling Technology; 4971), Cav1 (BD Biosciences; 610059), pacsin2 (Abgent; AP8088b); and cavin1 (Sigma; AV36965); for immunofluorescence, mouse monoclonal anti-cavin1 (BD Biosciences; 611258), goat polyclonal anti-EHD2 (Abcam; Ab23935), rabbit polyclonal anti-Cav1 (BD Biosciences; 610059), mouse monoclonal anti-lamin A/C (Santa Cruz Biotechnology; sc-7292), rabbit polyclonal anti-SUMO1 (Cell Signaling Technology; 4930), and rabbit polyclonal anti-SUMO2/3 (Cell Signaling Technology; 4971). Antibodies conjugated to Alexa Fluor 488, Cy3, Cy5, or HRP (Beckman Coulter and Invitrogen) were used as secondary antibodies. HaloTag dye JF635 was provided by L. Lavis (Janelia Research Campus, Howard Hughes Medical Institute, Ashburn, VA). Accutase was purchased from Sigma-Aldrich. Hepes, SDS, and Tris were purchased from Euromedex.

Plasmids

Cells were transfected using Lipofectamine 2000 (Invitrogen) according to the manufacturer's instructions. Experiments were performed 6–24 h after transfection. EHD2-mCherry, EHD2-EGFP, EHD2-I157Q-mCherry, and EHD2-T72A-mCherry were generously provided by A. Helenius (ETH Zurich, Zurich, Switzerland). EHD2-KK315-316AA-GFP was provided by M. Horowitz (Tel Aviv University, Tel Aviv, Israel). pmEmerald and Pacsin2-mCherry were purchased from Addgene. pCMV-HA-N was purchased from Clontech. EHD2-mEmerald was prepared by insertion of amplified EHD2 from EHD2-mCherry into pmEmerald plasmid using HindIII and BamHI restriction sites. Cav1-HaloTag was prepared by sequential insertion of Cav1 and HaloTag into pCMV-HA-N plasmid by EcoRI/BglII and XhoI/NotI restriction sites, respectively.

RNA interference

Cells were transfected with siRNAs using HiPerFect (Qiagen) according to the manufacturer's instructions and cultured for 72 h. Experiments were performed upon validation of depletion efficiency with immunoblot analysis using specific antibodies and normalization to the total level of CHC used as a loading control. Control siRNA (SI03650325, 5′-AAUUCUCCGAACGUGUCACGU-3′) was purchased from Qiagen and served as a reference point. The siRNA sequences were used at the final concentration of 20 nM: siEHD2 (Qiagen; SI04205271, 5′-AGCCCUUCCGCAAACUCAATT-3′, and SI04315108, 5′-CAUCCGUCAUUCAAATT-3′), siPacsin2 (Qiagen; SI02224292, 5′-CCCUUAAUGUCCCGAGCAATT-3′, and SI02224299, 5′-AGCUUUACAUAGAACCUUATT-3′), siFilamin pool of 4 FlexiTube GeneSolution (Qiagen; GS2316, 5′-GGAAGAAGAUCCAGCAGAATT-3′, 5′-GUGGCGAUGGCAUGUACAATT-3′, 5′-GGCCCAAACUGAACCCGAATT-3′, and 5′-CAGUCAACGAGGA-3′), siMOKA (GE Dharmacon; SMARTpool: ON-TARGETplus FBXO38 [81545] siRNA), siKLF7 (GE Dharmacon; SMARTpool: ON-TARGETplus KLF7 [8609] siRNA), and siCav1 (Eurogentec; 5′-CUAAACACCUCAACGAUGA-3′, 5′-GCAUCAACUUGCAGAAAGA-3′, 5′-GCAAAUACGUAGACUCGGA-3′, and 5′-GCAGUUGUACCAUGCAUUA-3′).

Cell culture

HeLa cells, Cav1-EGFP stably transfected HeLa cells (Sinha et al., 2011), and Hs578T cells were grown at 37°C under 5% CO_2 in DMEM GlutaMAX (GIBCO BRL Life Technologies) supple-

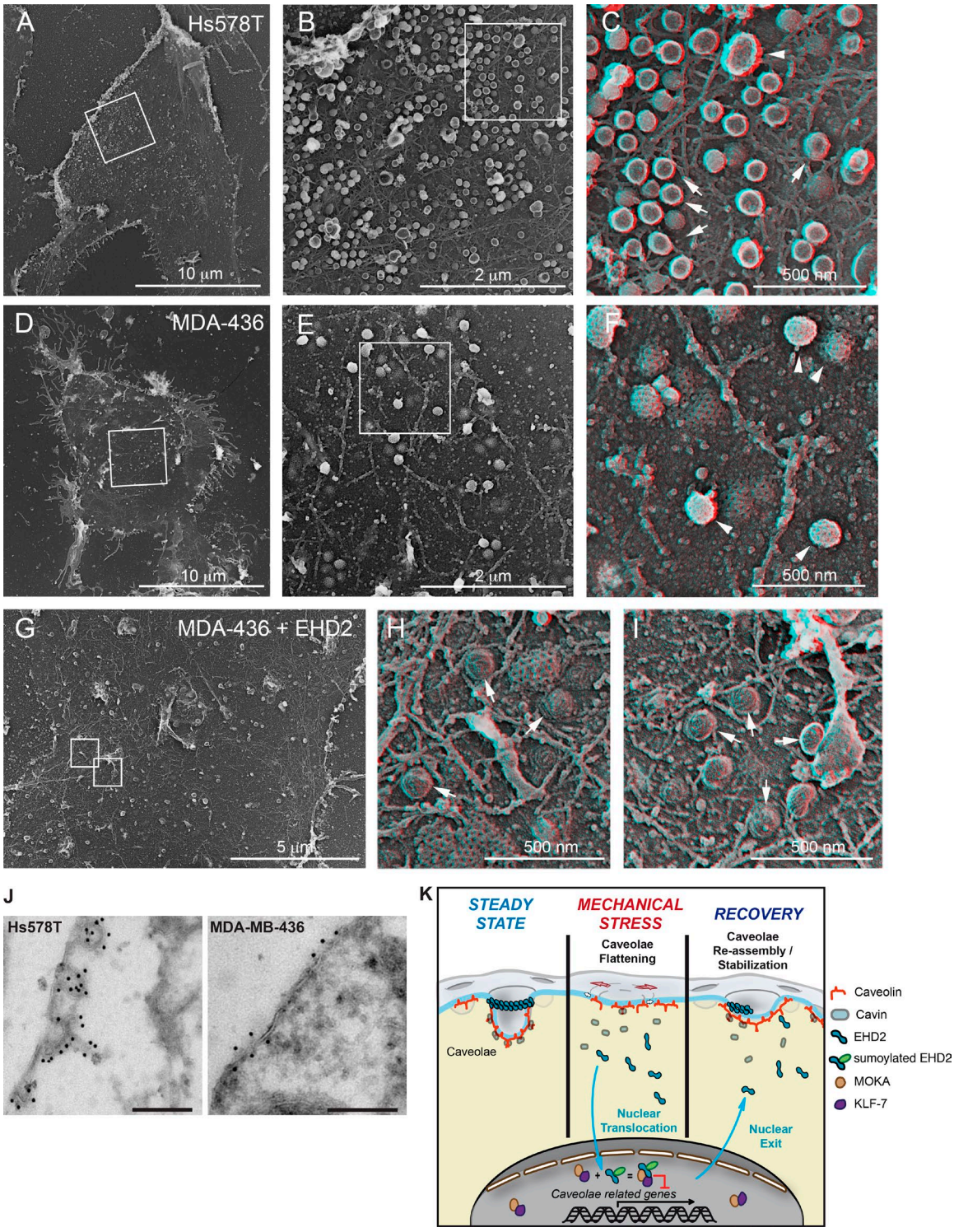

Figure 5. **EHD2 expression is required for the presence of caveolae at the plasma membrane of breast cancer cells. (A–I)** Survey view of the cytoplasmic surface of the plasma membrane in unroofed Hs578T cells (A–C), MDA-MB-436 (D–F) cells, and MDA-MB-436 cells transfected by EHD2-EGFP (G–I). For second inset (C, F, H, and I) use view glasses for 3D viewing of anaglyphs (left eye = red). Arrows indicate caveolae. Arrowheads indicate clathrin-coated pits. **(J)** Representative immunogold labeling of EM images of Cav1 protein localization in Hs578T and MDA-MB-436 cells. Scale bar = 200 nm. **(K)** Upon mechanical stress, Cav1, cavin1, and EHD2 are released from flattened caveolae. EHD2, but not cavin1 or Cav1, is SUMOylated and translocated to the nucleus where it controls gene transcription through interaction with MOKA and KLF-7. Upon stress release, EHD2 exits from the nucleus and is required for the stabilization of the caveolae reservoir at the plasma membrane.

mented with 10% FCS (GIBCO BRL Life Technologies), 5 mM pyruvate (GIBCO BRL Life Technologies), and 1% penicillin-streptomycin (GIBCO BRL Life Technologies). HeLa His-SUMO2 cells were grown as HeLa cells with 1 µg/ml puromycin (InvivoGen). MLECs (Sinha et al., 2011) were maintained in EGM-2 medium (Lonza) supplemented with 15% FBS (Hyclone; GE Healthcare), 4 mM L-glutamine (GIBCO BRL Life Technologies), 5 mM pyruvate, and 1% penicillin-streptomycin. MDA-MB-436 cells were grown at 37°C without CO_2 in Leibovitz's L-15 medium (GIBCO BRL Life Technologies) supplemented with 10% FCS (GIBCO BRL Life Technologies) and 1% penicillin-streptomycin (GIBCO BRL Life Technologies).

Generation of HeLa Cav1$^{-/-}$ cells

Single guide RNA (sgRNA) designed to target exon 3 of human caveolin-1 gene was selected and analyzed using online software Benchling. The selected guide (5′-GTATTTCGTCACAGTGAA GG-3′) was inserted into pSpCas9(BB)2A-Puro plasmid, which contains SpCas9 and sgRNA scaffold (px459 v2.0, Feng Zhang laboratory, Broad Institute of MIT and Harvard, Cambridge, MA; available from Addgene as plasmid 62988). 2 µg of plasmid was transfected using a single-cuvette Nucleofector device (Lonza) as per the manufacturer's protocol. In brief, 80% confluent HeLa cells were harvested, and 10^6 cells were resuspended in 100 µl complete solution R and transfected using Nucleofector program I-013. After transfection, cells were transferred to a 37°C, 5% CO_2 incubator, selected for puromycin for 72 h, and sorted as single cells into 96-well plates using a MoFlo Astrios cell sorter (Beckman Coulter). After clonal expansion, protein levels of clones were evaluated by Western immunoblotting.

Cyclic stretch

Cells were plated onto flexible-bottom plates (UniFlex plates; Flexcell International) coated with fibronectin (Sigma-Aldrich) and incubated at 37°C in a CO_2 incubator for 24 h before applying cyclic mechanical stretch. The cells were subjected to cyclic stretch at 0.5 Hz during 30 min using a computer-controlled vacuum stretch apparatus (FX-4000T Tension Plus System; FlexCell International) with a vacuum pressure sufficient to generate 10% mechanical stretch. Replicate control samples were maintained under static conditions with no applied cyclic stretch.

Hypo-osmotic shock

Hypo-osmotic shock was performed by diluting growth medium with deionized water (1:9 dilution for 30-mOsm hypo-osmotic shock and 1:1 for 150 mOsm hypo-osmotic shock).

Lysate preparation and immunoblot

Cells were lysed with sample buffer containing 2% SDS, 10% glycerol, 4 mM DTT, and Tris, pH 6.8. Lysates were analyzed by SDS-PAGE and immunoblotted with the indicated primary antibodies and HRP-conjugated secondary antibodies. Chemiluminescence signal was revealed using SuperSignal West Dura Extended Duration Substrate or SuperSignal West Femto Substrate (Thermo Fisher Scientific Life Technologies). Acquisition and quantification were performed on a ChemiDoc MP Imaging System (Bio-Rad).

Nuclear, cytosolic, and membrane extraction

Nuclear/cytoplasmic/membrane fractionation was conducted at resting conditions, at 2 and 5 min under hypo-osmotic shock (30 mOsm) as indicated, using the Subcellular Protein Fractionation Kit (Thermo Fisher Scientific) according to the manufacturer's protocol. The cytoplasmic fraction contains soluble cytoplasmic contents; the membrane fraction contains plasma, mitochondria, and ER/Golgi membranes; and the nuclear fraction contains the soluble nuclear extract and chromatin-bound nuclear proteins. Lysates were analyzed by SDS-PAGE and immunoblotted for lamin A/C as a marker of nuclear fraction, for Hsp90 as a marker of cytoplasmic fraction, and for CHC as a marker of membrane fraction. Fractions were quantified for protein content and normalized to the total cell lysate proteins.

GFP-trap

16 h after transfection, cells were treated with 100 nM leptomycin-B (Cell Signaling Technology; 9676) for 6 h. At resting conditions or after 5 min of hypo-osmotic shock, cells were harvested and lysed in 150 mM Tris-Cl, pH 6.7, 5% SDS, and 30% glycerol and then diluted 1:10 in PBS containing 0.5% NP-40 and protease inhibitor cocktail (Thermo Fisher Scientific). The lysates were then sonicated at 2× 10-s pulse (20 s in total) of 25% amplitude. Cleared lysates (13,200 rpm, 10 min, 4°C) were incubated overnight with GFPTrap-MA beads (Chromotek) at 4°C. Beads were washed three to five times with washing buffer (25 mM Tris-Cl, pH 7.4, 150 mM NaCl, 1 mM EDTA, and 5% glycerol) and eluted by boiling in 2× sample buffer at 95°C for 10 min. The eluted fractions were analyzed by Western blot and probed for GFP to determine the total EHD2-GFP pull-down level and for SUMO2/3 to measure SUMOylated EHD2.

Immunofluorescence and live-cell imaging

Cells were fixed for 15 min at room temperature with 4% PFA in PBS. After quenching with 50 mM NH_4Cl (Sigma-Aldrich) and permeabilization with 0.5% saponin (Sigma-Aldrich) or 1% Triton X-100, cells were blocked with 5% BSA (Sigma-Aldrich) and incubated sequentially with primary and secondary antibodies before being mounted in Fluoromount-G mounting medium (eBioscience). 2 µg/ml DAPI (Sigma-Aldrich) was used in mounting medium to counterstain nuclei. Images were acquired on a Leica DM 6000B inverted wide-field fluorescence microscope equipped with a HCX PL Apo 40× NA 1.25 oil-immersion objective and an EMCCD camera (Photometrics CoolSNAP HQ). Nuclear translocation was quantified with ImageJ software (National Institutes of Health) by calculating the nucleo-cytosolic ratio of EHD2 signal (nuclei masks were realized with the DAPI staining). TIRF images were acquired by TIRF video microscope (Nikon) equipped with a CFI Apo TIRF 100× NA 1.49 oil objective and an EMCCD camera (Photometrics HQ2). The quantification of surface Cav1 spots was realized by LabView as described in Sinha et al. (2011). In brief, caveolae were detected from TIRF images by first applying on the raw image a local intensity threshold of window size varying from 8 × 8 to 64 × 64 pixels, depending on the quality of the image. Pixels clustering together were detected as particles depending on their connectivity. Holes within particles, if any, were filled, connected particles were disconnected

by eroding boundaries, and finally particles were selected by size. For colocalization, images were analyzed with ImageJ and the JACoP plugin (Bolte and Cordelières, 2006). For live imaging, cells were maintained at 37°C and under 5% CO_2 throughout the acquisition.

Lattice light sheet microscopy (LLSM) imaging and intensity analysis

Cells expressing Cav1-HaloTag and EHD2-mEmerald were imaged using LLSM (Chen et al., 2014). Image volumes of Cav1-HaloTag– and EHD2-mEmerald–labeled cells were recorded every 2 s, using a 10-ms exposure in 30 mOsm hypo-osmotic environment for a total time of 5 min. All 3D datasets acquired were deskewed to account for the 31.8° angle of the detection objective (Nikon). After deskewing, deconvolution was performed using the Richardson–Lucy algorithm, and 4D visualization was performed using Vision 4D software (Arivis). Intensity analysis is based on a custom script written in Matlab, using Image Processing Toolbox. For the segmentation algorithm, nucleus and cell masks were defined based on Cav1 deconvolved images. The cell contour for each time point and z-plane was calculated using Otsu (Otsu, 1979) and Chan–Vese (Chan and Vese, 2001) algorithms implemented in Matlab Image Processing Toolbox. Similar analysis was performed to estimate the nucleus contour. Intensity for each time point was calculated by integrating the defined cell and nucleus area of the deskewed images for all planes of EHD2 labeling. The ratio between nucleus and whole-cell intensity was estimated for each time point and fitted to a sigmoid equation in Prism software.

PLA

The PLA kit was purchased from Sigma-Aldrich, and the assay was performed according to the manufacturer's protocol. Cells were fixed in 4% PFA for 10 min at room temperature, quenched in 50 mM NH_4Cl for 10 min, permeabilized with 0.2% Triton X-100 (wt/vol) for 10 min, and blocked in PBS/BSA. Cells were incubated with primary antibodies for 45 min in PBS/BSA. Coverslips were mounted in Fluoromount with DAPI to stain nuclei. PLA signals were visible as fluorescent dots and imaged using wide-field fluorescence inverted microscope Leica DM 6000B equipped with a HCX PL Apo 63× NA 1.32 oil-immersion objective and an EMCCD camera (Photometrics CoolSNAP HQ). Fluorescent dots were quantified using ImageJ. Cells and nuclei were delineated to create masks. After a maximum entropy threshold, the PLA dots were quantified in both masks with the ImageJ Analyze Particles plugin. Cytoplasmic and plasma membrane values were obtained by subtracting nuclear count from the cellular count. All counts were divided by the area in pixels.

qPCR

Cells were lysed using RNeasy Plus extraction kit from Qiagen at steady state or after 30 min of cyclic stretch. For hypo-osmotic shock experiments, cells were first exposed to 30 mOsm medium for 5 min, moved into iso-osmotic medium at 37°C during 1 h, and finally lysed using RNeasy Plus extraction kit. Reverse transcription reaction was performed with 1,000 ng total RNA per reaction using high-capacity cDNA reverse transcription kit (Applied Biosystems). qPCR was performed using 50 ng cDNA per 20-µl reaction. TaqMan Gene Expression Assays from Applied Biosystems were used: GAPDH (Hs02758991_g1), Cav1 (Hs00971716_m1), Cav2 (Hs00184597_m1), Cavin1 (Hs00396859_m1), Cavin2 (Hs00190538_m1), EHD2 (Hs00907482_m1), and Flot1 (Hs00195134_m1). Relative expression levels were calculated using ΔΔCT method with fold changes calculated as $2^{-\Delta\Delta CT}$. GAPDH served as the internal control.

DNA microarray

Total RNA was isolated using RNeasy Plus extraction kit after 30 min of cyclic stretch at 0.5 Hz. Gene expression profiling was performed using Affymetrix Human Gene ST 2.1 arrays. Cel files were preprocessed and annotated using the oligo and clariomshumanhttranscriptcluster.db packages. Normalization of expression across chips was performed using the RMA algorithm (rma() function from oligo package). No outlier was observed after visual inspection using the hist() and boxplot() functions. For each condition, the mean log2 fold change (logFC) compared with control was computed using the Limma R package. These logFC tables were then used to perform GSEA (Subramanian et al., 2005) with default parameters using the GSEA java application (v.2.2.1) and the gene set databases available on http://software.broadinstitute.org/gsea/msigdb/. Analysis was performed using the GseaPreranked tool. Enrichments were considered significant if the corresponding false discovery rate (FDR; BH correction) was lower than 5%. Data description, raw data files, and tables for logFC and FDR values have been deposited on http://microarrays.curie.fr/.

Force measurements

Plasma membrane tethers were extracted from cells with a bead (3 µm in diameter; Polysciences) coated with concanavalin A (Sigma-Aldrich) trapped in optical tweezers. The optical tweezers are made of a 1,064-nm laser beam (ytterbium fiber laser, λ = 1064 nm, TEM 00, 5 W; IPG Photonics) expanded and steered (optics by Elliot Scientific) in the back focal plane of the microscope objective (Apo-TIRF 100×, NA 1.45; Nikon). The whole setup was mounted on a Nikon Eclipse-Ti inverted microscope. The sample was illuminated by transmitted light, and videos were acquired at 10 Hz with an EMCCD camera (iXon 897; Andor) driven by Micro-Manager (Edelstein et al., 2014). The fine movements and particularly the translational movement necessary to pull the membrane tether were performed using a custom-made stage mounted on a piezoelectric element (P753; Physik Instrumente) driven by a servo controller (E665; Physik Instrumente) and a function generator (Tektronix AFG320; Sony).

Calibration was performed using an oscillatory modulation driven by a function generator (Tolić-Nørrelykke et al., 2006) and measuring the response of the bead to an oscillatory motion of the stage. We measured $k = 22P$ pN/(µm · W), where P is the laser power. This relationship is linear in the laser power range used for the experiments (0.5–2 W).

The membrane tether was held at constant length to measure the static force. For measuring membrane tension changes due to hypo-osmotic shock, the tether was held while the medium was diluted until the osmolarity reached 150 mOsm. For assessing the membrane tension change during recovery, medium osmolarity

was adjusted back to 300 mOsm with 10× MEM (GIBCO BRL Life Technologies). The medium changes were performed by slowly flowing in water or 10× MEM using a 2-ml surgical syringe. The position of the beads used to compute tether forces was detected from the images using a custom ImageJ macro.

EM

Cells were fixed at 37°C with 2% PFA in 0.1 M phosphate buffer. After several washes and quenching with glycine, cells were harvested in 10% gelatin, pelleted by mild centrifugation, and incubated on ice for 2 h. Afterward, pelleted cells were incubated overnight at 4°C in 2.3 M sucrose and mounted on nails in liquid nitrogen. 65-nm ultrathin cryosections were obtained using a Leica UCT ultracryomicrotome and collected on Cu/Pd-formvar-carbon–coated grids by picking up in a 1:1 mix of 2.3 M sucrose and methylcellulose. The sections were processed for immunogold labeling with an anti-Cav1 polyclonal antibody and Protein A conjugated to 10 nm gold (PAG10; https://www.cellbiology-utrecht.nl/) as reported previously (Sinha et al., 2011). After each labeling, grids were extensively washed with PBS and fixed again with 1% glutaraldehyde for 5 min at room temperature. Contrast was obtained by incubation with a 9:1 mix of methylcellulose and 4% uranyl acetate in water. Electron micrographs were acquired on a Tecnai Spirit electron microscope (FEI) equipped with a 4k CCD camera (EMSIS).

For unroofed metal replica EM, adherent plasma membranes from cultured cells grown on glass coverslips were disrupted by sonication as described previously (Heuser, 2000). Sample processing for platinum-replica EM of unroofed cells was performed as follows: glutaraldehyde/paraformaldehyde-fixed cells were further sequentially treated with osmium tetroxide, tannic acid, and uranyl acetate before ethanol dehydration and hexamethyldisilazane drying (Sigma-Aldrich). Dried samples were then rotary-shadowed with ∼2 nm platinum and 8 nm carbon. The resultant platinum replica was floated off the glass by angled immersion into hydrofluoric acid (5%), washed several times by flotation on distilled water, and picked up on 200-mesh formvar/carbon-coated EM grids. The grids were mounted in a eucentric side-entry goniometer stage of a transmission electron microscope operated at 80 kV (model CM120; Philips), replicas were viewed at ±10° tilt angles, and images were recorded with a Morada digital camera (Olympus). Images were processed in Adobe Photoshop to adjust brightness and contrast and presented in inverted contrast. Anaglyphs were made by converting the −10° tilt image to red and the +10° tilt image to cyan (blue/green), layering them on top of each other using the screen blending mode in Adobe Photoshop, and aligning them to each other.

Statistical analyses

All analyses were performed using GraphPad Prism v.6.0 and 7.0 for Windows (GraphPad Software). Two-tailed *t* test was used if comparing only two conditions. For comparing more than two conditions, one-way ANOVA was used with Bonferroni's multiple comparison test or Dunnett's multiple comparison test (if comparing all conditions to the control condition). Significance of mean comparison is marked on the graphs by asterisks. Error bars denote SEM or SD.

Online supplemental material

Fig. S1 shows imaging and quantification of EHD2 nuclear translocation under hypo-osmotic shock. Fig. S2 shows TIRF imaging and quantification of the dynamic colocalization of Cav1 and EHD2 during osmotic shock (A), EHD2-SUMO1 interaction by PLA (B), and EHD2-dependent gene regulation under hypo-osmotic conditions (C). Fig. S3 shows TIRF imaging and quantification of Cav1 spots after hypo-osmotic shock and recovery (A–C) and RNA silencing efficiency (D). Video 1 shows LLSM imaging EHD2 nuclear translocation under hypo-osmotic shock in a HeLa cell.

Acknowledgments

We thank Thierry Dubois for providing materials and expertise, Pierre Sens for analysis of membrane tension measurements, and Audrey Rapinat and David Gentien from the Genomics platform of the Institut Curie for the microarrays analysis. We are grateful to Michaël Trichet at the Electron Microscopy facility of the Institut de Biologie Paris-Seine (IBPS) for helpful advice and access to metal coaters.

The facilities as well as scientific and technical assistance from the PICT-IBiSA/Nikon Imaging Centre staff at Institut Curie-Centre National de la Recherche Scientifique and the France-BioImaging infrastructure (Agence Nationale de la Recherche [ANR], ANR-10-INSB-04) are acknowledged. LLSM was performed at the Advanced Imaging Center (AIC) at Howard Hughes Medical Institute Janelia Research Campus. The AIC is jointly supported by the Gordon and Betty Moore Foundation and Howard Hughes Medical Institute. The electron microscope facility was supported by the ANR through "Investments for the Future" program (France-BioImaging, ANR-10-INSB-04). This work was supported by institutional grants from the Institut Curie, Institut National de la Santé et de la Recherche Médicale, and Centre National de la Recherche Scientifique, and by specific grants from ANR (MECANOCAV, ANR-12-BSV2-0011; DECAV-RECAV, ANR-14-CE09-0008-03; and MOTICAV, ANR-17-CE-0013), Institut National du Cancer (INCa PLBIO12-203), Fondation de France, Marie Curie Actions—Networks for Initial Training (H2020-MSCA-ITN-2014), Association Française contre les Myopathies (15717 and 16754), and Program labellisé, Fondation ARC pour la Recherche sur le Cancer (PGA1 RF20170205456) to C. Lamaze, ANR (ANR-14-CE14-0002-02), Human Frontier Science Program (RGP0029-2014), and European Research Council (advanced grant 340485) to L. Johannes, ANR young researcher grant (EndoMechano ANR-14-CE12-0001-01) to S. Vassilopoulos. A. Grassart is supported by a Pasteur-Roux Fellowship. P. Pierobon is supported by grants from ANR (ANR-10-JCJC-1504-Immuphy) and PIC (Programme Incitatif et Collaboratif) Curie, "Cell polarity, division, growth and cancer." S. Torrino and W.-W. Shen were supported by a postdoctoral fellowship from Fondation ARC pour la Recherche sur le Cancer and Fondation de France, respectively. D. Köster and W.-W. Shen were supported by the Labex CelTisPhyBio Grants Program. The Johannes and Lamaze teams, the PICT-IBiSA/Nikon Imaging Centre at Institut Curie-Centre National de la Recherche Scientifique, and the France-BioImaging infrastructure are members of Labex CelTisPhyBio (ANR, ANR-

10-LBX-0038) and of Initiatives d'Excellence (IDEX) PSL (ANR, ANR-10-IDEX-0001-02 PSL).

The authors declare no competing financial interests.

Author contributions: S. Torrino and W.-W. Shen designed and performed the experiments, analyzed results and wrote the manuscript. C.M. Blouin, S.K. Mani, C. Viaris de Lesegno, P. Bost, D. Köst, C.A. Valades-Cruz, V. Chambon, and S. Vassilopoulos performed experiments or analysis. C.M. Blouin, A. Grassart, P. Pierobon, L. Johannes, V. Soumelis, C. Coirault, and S. Vassilopoulos provided technical support and conceptual advice. C. Lamaze supervised the project, designed experiments, and wrote the manuscript.

Submitted: 19 January 2018
Revised: 4 July 2018
Accepted: 27 September 2018

References

Ariotti, N., M.A. Fernández-Rojo, Y. Zhou, M.M. Hill, T.L. Rodkey, K.L. Inder, L.B. Tanner, M.R. Wenk, J.F. Hancock, and R.G. Parton. 2014. Caveolae regulate the nanoscale organization of the plasma membrane to remotely control Ras signaling. *J. Cell Biol.* 204:777–792. https://doi.org/10.1083/jcb.201307055

Bolte, S., and F.P. Cordelières. 2006. A guided tour into subcellular colocalization analysis in light microscopy. *J. Microsc.* 224:213–232. https://doi.org/10.1111/j.1365-2818.2006.01706.x

Chan, T.F., and L.A. Vese. 2001. Active contours without edges. *IEEE Trans. Image Process.* 10:266–277. https://doi.org/10.1109/83.902291

Chen, B.C., W.R. Legant, K. Wang, L. Shao, D.E. Milkie, M.W. Davidson, C. Janetopoulos, X.S. Wu, J.A. Hammer III, Z. Liu, et al. 2014. Lattice light-sheet microscopy: imaging molecules to embryos at high spatiotemporal resolution. *Science.* 346:1257998. https://doi.org/10.1126/science.1257998

Cheng, J.P., C. Mendoza-Topaz, G. Howard, J. Chadwick, E. Shvets, A.S. Cowburn, B.J. Dunmore, A. Crosby, N.W. Morrell, and B.J. Nichols. 2015. Caveolae protect endothelial cells from membrane rupture during increased cardiac output. *J. Cell Biol.* 211:53–61. https://doi.org/10.1083/jcb.201504042

DuFort, C.C., M.J. Paszek, and V.M. Weaver. 2011. Balancing forces: architectural control of mechanotransduction. *Nat. Rev. Mol. Cell Biol.* 12:308–319. https://doi.org/10.1038/nrm3112

Edelstein, A.D., M.A. Tsuchida, N. Amodaj, H. Pinkard, R.D. Vale, and N. Stuurman. 2014. Advanced methods of microscope control using μManager software. *J. Biol. Methods.* 1:e10. https://doi.org/10.14440/jbm.2014.36

Enserink, J.M. 2015. Sumo and the cellular stress response. *Cell Div.* 10:4. https://doi.org/10.1186/s13008-015-0010-1

Fernández-Sánchez, M.E., S. Barbier, J. Whitehead, G. Béalle, A. Michel, H. Latorre-Ossa, C. Rey, L. Fouassier, A. Claperon, L. Brullé, et al. 2015. Mechanical induction of the tumorigenic β-catenin pathway by tumour growth pressure. *Nature.* 523:92–95. https://doi.org/10.1038/nature14329

Gambin, Y., N. Ariotti, K.A. McMahon, M. Bastiani, E. Sierecki, O. Kovtun, M.E. Polinkovsky, A. Magenau, W. Jung, S. Okano, et al. 2013. Single-molecule analysis reveals self assembly and nanoscale segregation of two distinct cavin subcomplexes on caveolae. *eLife.* 3:e01434. https://doi.org/10.7554/eLife.01434

Garcia, J., J. Bagwell, B. Njaine, J. Norman, D.S. Levic, S. Wopat, S.E. Miller, X. Liu, J.W. Locasale, D.Y.R. Stainier, and M. Bagnat. 2017. Sheath cell invasion and trans-differentiation repair mechanical damage caused by loss of caveolae in the zebrafish notochord. *Curr. Biol.* 27:1982–1989.e3. https://doi.org/10.1016/j.cub.2017.05.035

Geiss-Friedlander, R., and F. Melchior. 2007. Concepts in sumoylation: a decade on. *Nat. Rev. Mol. Cell Biol.* 8:947–956. https://doi.org/10.1038/nrm2293

Gervásio, O.L., W.D. Phillips, L. Cole, and D.G. Allen. 2011. Caveolae respond to cell stretch and contribute to stretch-induced signaling. *J. Cell Sci.* 124:3581–3590. https://doi.org/10.1242/jcs.084376

Goetz, J.G., P. Lajoie, S.M. Wiseman, and I.R. Nabi. 2008. Caveolin-1 in tumor progression: the good, the bad and the ugly. *Cancer Metastasis Rev.* 27:715–735. https://doi.org/10.1007/s10555-008-9160-9

Heuser, J. 2000. The production of 'cell cortices' for light and electron microscopy. *Traffic.* 1:545–552. https://doi.org/10.1034/j.1600-0854.2000.010704.x

Hoernke, M., J. Mohan, E. Larsson, J. Blomberg, D. Kahra, S. Westenhoff, C. Schwieger, and R. Lundmark. 2017. EHD2 restrains dynamics of caveolae by an ATP-dependent, membrane-bound, open conformation. *Proc. Natl. Acad. Sci. USA.* 114:E4360–E4369. https://doi.org/10.1073/pnas.1614066114

Iskratsch, T., H. Wolfenson, and M.P. Sheetz. 2014. Appreciating force and shape—the rise of mechanotransduction in cell biology. *Nat. Rev. Mol. Cell Biol.* 15:825–833. https://doi.org/10.1038/nrm3903

Joshi, B., M. Bastiani, S.S. Strugnell, C. Boscher, R.G. Parton, and I.R. Nabi. 2012. Phosphocaveolin-1 is a mechanotransducer that induces caveola biogenesis via Egr1 transcriptional regulation. *J. Cell Biol.* 199:425–435. https://doi.org/10.1083/jcb.201207089

Kovtun, O., V.A. Tillu, W. Jung, N. Leneva, N. Ariotti, N. Chaudhary, R.A. Mandyam, C. Ferguson, G.P. Morgan, W.A. Johnston, et al. 2014. Structural insights into the organization of the cavin membrane coat complex. *Dev. Cell.* 31:405–419. https://doi.org/10.1016/j.devcel.2014.10.002

Lamaze, C., and S. Torrino. 2015. Caveolae and cancer: A new mechanical perspective. *Biomed. J.* 38:367–379. https://doi.org/10.4103/2319-4170.164229

Lamaze, C., N. Tardif, M. Dewulf, S. Vassilopoulos, and C.M. Blouin. 2017. The caveolae dress code: structure and signaling. *Curr. Opin. Cell Biol.* 47:117–125. https://doi.org/10.1016/j.ceb.2017.02.014

Li, M., X. Yang, J. Zhang, H. Shi, Q. Hang, X. Huang, G. Liu, J. Zhu, S. He, and H. Wang. 2013. Effects of EHD2 interference on migration of esophageal squamous cell carcinoma. *Med. Oncol.* 30:396. https://doi.org/10.1007/s12032-012-0396-4

Lim, Y.W., H.P. Lo, C. Ferguson, N. Martel, J. Giacomotto, G.A. Gomez, A.S. Yap, T.E. Hall, and R.G. Parton. 2017. Caveolae protect notochord cells against catastrophic mechanical failure during development. *Curr. Biol.* 27:1968–1981.e7. https://doi.org/10.1016/j.cub.2017.05.067

Liu, J., W. Ni, L. Qu, X. Cui, Z. Lin, Q. Liu, H. Zhou, and R. Ni. 2016. Decreased Expression of EHD2 Promotes Tumor Metastasis and Indicates Poor Prognosis in Hepatocellular Carcinoma. *Dig. Dis. Sci.* 61:2554–2567. https://doi.org/10.1007/s10620-016-4202-6

Lo, H.P., S.J. Nixon, T.E. Hall, B.S. Cowling, C. Ferguson, G.P. Morgan, N.L. Schieber, M.A. Fernandez-Rojo, M. Bastiani, M. Floetenmeyer, et al. 2015. The caveolin-cavin system plays a conserved and critical role in mechanoprotection of skeletal muscle. *J. Cell Biol.* 210:833–849. https://doi.org/10.1083/jcb.201501046

Ludwig, A., G. Howard, C. Mendoza-Topaz, T. Deerinck, M. Mackey, S. Sandin, M.H. Ellisman, and B.J. Nichols. 2013. Molecular composition and ultrastructure of the caveolar coat complex. *PLoS Biol.* 11:e1001640. https://doi.org/10.1371/journal.pbio.1001640

Morén, B., C. Shah, M.T. Howes, N.L. Schieber, H.T. McMahon, R.G. Parton, O. Daumke, and R. Lundmark. 2012. EHD2 regulates caveolar dynamics via ATP-driven targeting and oligomerization. *Mol. Biol. Cell.* 23:1316–1329. https://doi.org/10.1091/mbc.e11-09-0787

Nassar, Z.D., and M.O. Parat. 2015. Cavin Family: New Players in the Biology of Caveolae. *Int. Rev. Cell Mol. Biol.* 320:235–305. https://doi.org/10.1016/bs.ircmb.2015.07.009

Nassoy, P., and C. Lamaze. 2012. Stressing caveolae new role in cell mechanics. *Trends Cell Biol.* 22:381–389. https://doi.org/10.1016/j.tcb.2012.04.007

Otsu, N. 1979. Threshold Selection Method from Gray-Level Histograms. *IEEE Trans. Syst. Man Cybern.* 9:62–66. https://doi.org/10.1109/TSMC.1979.4310076

Palade, G.E. 1953. The fine structure of blood capillaries. *J. Appl. Phys.* 24:1424.

Pekar, O., S. Benjamin, H. Weidberg, S. Smaldone, F. Ramirez, and M. Horowitz. 2012. EHD2 shuttles to the nucleus and represses transcription. *Biochem. J.* 444:383–394. https://doi.org/10.1042/BJ20111268

Sheetz, M.P. 2001. Cell control by membrane-cytoskeleton adhesion. *Nat. Rev. Mol. Cell Biol.* 2:392–396. https://doi.org/10.1038/35073095

Shi, Y., X. Liu, Y. Sun, D. Wu, A. Qiu, H. Cheng, C. Wu, and X. Wang. 2015. Decreased expression and prognostic role of EHD2 in human breast carcinoma: correlation with E-cadherin. *J. Mol. Histol.* 46:221–231. https://doi.org/10.1007/s10735-015-9614-7

Sinha, B., D. Köster, R. Ruez, P. Gonnord, M. Bastiani, D. Abankwa, R.V. Stan, G. Butler-Browne, B. Vedie, L. Johannes, et al. 2011. Cells respond to mechanical stress by rapid disassembly of caveolae. *Cell.* 144:402–413. https://doi.org/10.1016/j.cell.2010.12.031

Söderberg, O., M. Gullberg, M. Jarvius, K. Ridderstråle, K.J. Leuchowius, J. Jarvius, K. Wester, P. Hydbring, F. Bahram, L.G. Larsson, and U. Landegren. 2006. Direct observation of individual endogenous protein complexes in situ by proximity ligation. *Nat. Methods.* 3:995–1000. https://doi.org/10.1038/nmeth947

Stoeber, M., I.K. Stoeck, C. Hänni, C.K. Bleck, G. Balistreri, and A. Helenius. 2012. Oligomers of the ATPase EHD2 confine caveolae to the plasma membrane through association with actin. *EMBO J.* 31:2350–2364. https://doi.org/10.1038/emboj.2012.98

Stoeber, M., P. Schellenberger, C.A. Siebert, C. Leyrat, A. Helenius, and K. Grünewald. 2016. Model for the architecture of caveolae based on a flexible, net-like assembly of Cavin1 and Caveolin discs. *Proc. Natl. Acad. Sci. USA.* 113:E8069–E8078. https://doi.org/10.1073/pnas.1616838113

Subramanian, A., P. Tamayo, V.K. Mootha, S. Mukherjee, B.L. Ebert, M.A. Gillette, A. Paulovich, S.L. Pomeroy, T.R. Golub, E.S. Lander, and J.P. Mesirov. 2005. Gene set enrichment analysis: a knowledge-based approach for interpreting genome-wide expression profiles. *Proc. Natl. Acad. Sci. USA.* 102:15545–15550. https://doi.org/10.1073/pnas.0506580102

Tolić-Nørrelykke, S.F., M.B. Rasmussen, F.S. Pavone, K. Berg-Sørensen, and L.B. Oddershede. 2006. Stepwise bending of DNA by a single TATA-box binding protein. *Biophys. J.* 90:3694–3703. https://doi.org/10.1529/biophysj.105.074856

Yamada, E. 1955. The fine structure of the gall bladder epithelium of the mouse. *J. Biophys. Biochem. Cytol.* 1:445–458. https://doi.org/10.1083/jcb.1.5.445

Yang, X., H. Ren, L. Yao, X. Chen, and A. He. 2015. Role of EHD2 in migration and invasion of human breast cancer cells. *Tumour Biol.* 36:3717–3726. https://doi.org/10.1007/s13277-014-3011-9

Yeow, I., G. Howard, J. Chadwick, C. Mendoza-Topaz, C.G. Hansen, B.J. Nichols, and E. Shvets. 2017. EHD Proteins Cooperate to Generate Caveolar Clusters and to Maintain Caveolae during Repeated Mechanical Stress. *Curr. Biol.* 27:2951–2962.e5. https://doi.org/10.1016/j.cub.2017.07.047